Three-dimensional visualization of the microstructure development of Sr-modified Al-15Si casting alloy using FIB-EsB tomography

M. Timpel[a,*], N. Wanderka[a], B.S. Murty[b], J. Banhart[a]

[a] *Helmholtz-Zentrum Berlin für Materialien und Energie GmbH, Hahn-Meitner-Platz 1, D-14109 Berlin, Germany*

[b] *Department of Metallurgical and Materials Engineering, Indian Institute of Technology Madras, Chennai 600 036, India*

Abstract

Unmodified and Sr-modified (after 5 and 120 minutes of melt holding) Al-15Si alloys were investigated by transmission electron microscopy and focused ion beam tomography using energy selective backscattered electrons for imaging. The three-dimensional visualization of the microstructure provided not only the true morphology of the Al-Si eutectic and Fe-rich intermetallics, but also allowed us to estimate their volume fractions. The evolution of Fe-rich α-phase morphology in the unmodified alloy proceeded during eutectic growth according to a model proposed. In the unmodified alloy, only Fe-rich α-phase was found, whereas in the Sr-modified alloy after 5 minutes of melt holding, two morphologies of Fe-rich phases were observed, namely a Fe-rich α-phase and a Fe-rich δ-phase. Both phases segregated mainly at modified eutectic grain boundaries. After 120 minutes of melt holding, the eutectic microstructure is similar to the unmodified structure again and only

*Corresponding author

Email address: melanie.timpel@helmholtz-berlin.de (M. Timpel)

the Fe-rich α-phase could be observed in this case.
Keywords:
FIB-EsB tomography, Al-Si alloys, Sr modification, Intermetallic compounds, Microstructure

1. Introduction

The eutectic modification of Al-Si alloys is very important, primarily to improve mechanical properties of cast materials [1]. Additions of Sr, Na or several rare earth elements to Al-Si alloys result in a transformation of the eutectic Si from coarse plate-like morphology to a fine fibrous structure [2–4]. Modification not only affects the morphology of the eutectic Si but also the development of intermetallic phases formed by impurities during solidification. In Al-Si foundry alloys the most common impurity element is Fe. Different Fe-rich intermetallics, including α-Al_8Fe_2Si or -$Al_{15}(Fe,Mn)_3Si_2$, β-Al_5FeSi, δ-Al_4FeSi_2 and π-$Al_8Mg_3FeSi_6$ have been identified in Al-Si casting alloys, strongly depending on the composition of the alloy [5–7]. However, the effect of the addition of Sr on the formation of Fe-rich intermetallics in foundry alloys is still not well understood [8–12].

Iron-rich intermetallics appear in different morphologies such as 'polyhedral', so-called 'Chinese script' or 'needle-shaped' in two-dimensional (2D) micrographs that are projections of their true shape. In order to obtain the true shape of eutectic or intermetallic phases, a three-dimensional (3D) reconstruction based on many 2D images is necessary. Recently, a qualitative tomographic analysis of eutectic morphologies based on metallographic 2D optical images with a resolution of about 2 μm in the slicing direction has been reported [13, 14]. A characterization of eutectic Si with a much higher resolution of about 60 nm in the image plane and 300 nm in depth was recently achieved using serial sectioning with a focused ion beam (FIB) combined with energy dispersive X-ray spectroscopy (EDX) [15]. Nevertheless, only few tomographic investigations have been performed on the Al-Si eutectic [13–15]. A 3D visualization of the eutectic microstructure at even smaller length scales is still urgently needed to reveal even finer phase distributions and to characterize their morphologies.

In the present study, focused ion beam-energy selective backscattered (FIB-EsB) tomography has been performed in order to obtain information on the nanoscale with compositional contrast by high-angle backscattered electrons. Compared to similar FIB-EDX tomography techniques [15, 16], FIB-EsB tomography provides not only 3D information within a volume larger than 1000 μm^3 but also high resolution of a few tens of nanometers in the lateral direction and of the order of 50 nm in the FIB slicing direction. The 3D eutectic microstructure in unmodified and Sr-modified Al-Si alloys has been visualized with its entire constitution of binary Al-Si eutectic and intermetallic impurity phases. Moreover, their morphologies were obtained and their size and volume fractions estimated. Structure and chemical composition of intermetallic phases were also studied by transmission electron microscopy (TEM).

2. Experimental

2.1. Alloy preparation

Hypereutectic Al-15 wt%Si alloy has been prepared using pure Al (99.7%) and a Al-30 wt%Si master alloy. This alloy composition was chosen because it contains a large volume fraction of eutectic, which facilitates the investigation of the eutectic microstructure. For studies of modification, 500 g of Al-15Si alloy were melted under a cover flux (45% NaCl + 45% KCl + 10% NaF) in zirconia-coated graphite crucibles in a furnace where the melt was held at 720°C. After degassing with hexachloroethane, the Al-10 wt%Sr master alloy chips were added to the melt for modification. After adding the modifier the melt was stirred for 30 s with a zirconia coated graphite rod, after which no further stirring was carried out. A part of the melt was poured into a cylindrical graphite mold (25 mm diameter and 100 mm height) after 5 and 120 min of melt holding. The average cooling rate prior to the start of the first solidification was 6.5 K/s. The sample designation 'unmodified' refers to that part of the alloy melt that was cast before the addition of the modifier. The chemical compositions of the unmodified and the two Sr-modified Al-15Si alloy castings were determined by inductively coupled plasma-atomic emission spectroscopy (ICP-AES), see Table 1.

2.2. Microstructural characterization

The cast rods were sectioned perpendicular to their axes, ground using standard metallographic procedures and finally polished with a colloidal silica suspension of 0.05 μm particle diameter. All specimens investigated in the present study were extracted from the centers of the castings 15 mm from the lower end of the ingot. The microstructure was investigated using optical microscopy, combined FIB with scanning electron microscopy (SEM), and TEM. Samples for optical microscopy were etched for 30 s at 20°C in a mixture of 60 ml water, 10 g sodium hydroxide and 5 g potassium ferricyanide in order to improve contrast [17].

A Zeiss 1540EsB CrossBeam® workstation combining an ultra-high resolution GEMINI® field emission column with the high performance Canion gallium ion column was used for characterizing the alloys. The instrument is equipped with a NORAN EDX detector from Thermo Scientific.

FIB serial sectioning and SEM imaging for tomography was performed using a method similar to that described in Ref. 18. A 30 keV Ga ion beam of 500 pA ion current was used for FIB milling. During serial sectioning, layers of about 50 nm were removed in each step. High-resolution imaging of 2D slices was performed using an in-column energy selective backscattered (EsB) electron detector with an acceleration voltage of 2 kV and a grid voltage of -1.5 kV. The elastically backscattered high-angle electrons give rise to a high-resolution, compositionally weighted signal with minimal topographic contrast. Recursive alignment of the image stack was carried out using the software 'ImageJ' with the plugin *stackreg* [19]. Volume segmentation was carried out by chosing suitable gray levels applying global thresholding. After processing with a median filter, 3D visualization of the structures and volume fraction analysis was performed using the software 'VGStudio MAX 2.0'.

For TEM, samples of 1x1 mm^2 area were mechanically ground to about 10 μm thickness using the T-tool technique [20], after which they were finally Ar-ion thinned with a voltage of 5 kV, a current of 2.5 mA and an angle of incidence of $\pm$ 6° in a Bal-Tec Res101 broad ion beam thinner. TEM analysis of the microstructure was carried out using a Philips CM30 microscope operating at 300 kV equipped with an EDAX Genesis EDX system. In order to identify the intermetallic impurity phases present in the investigated alloys unambiguously, the crystal structures of the Fe-rich intermetallics were determined by selected area electron diffraction (SAED) patterns. The chemical composition of the constituent phases was analyzed by TEM-EDX using a minimum of five measurements for each Fe-rich intermetallic phase.

3. Results

3.1. Microstructural features

Figure 1 shows optical micrographs of the cast alloy (a) without modifier and with addition of Sr (b) after 5 min and (c) after 120 min of melt holding. The microstructure of the unmodified alloy shown in Fig. 1(a) consists of polyhedral Si crystals, surrounded by a halo of coarse primary Al phases. Beside the primary phases, lamellar plates of eutectic Si embedded in an Al matrix are obtained as well. Despite etching the sample surface for contrast enhancement, no clear distinction could be made between the unmodified Al-Si eutectic and other intermetallic phases. The microstructure of the Sr-modified alloy after 5 min of melt holding is shown in Fig. 1(b). The size of the primary Si crystals is larger here, whereas their number per unit area is reduced. The eutectic microstructure is partially altered and consists of unmodified regions (region A) as well as modified regions with more rounded eutectic Si particles (region B). For the Sr-modified alloy after 5 min of melt holding, eutectic grain boundaries and intermetallic phases (region C) have been enhanced by etching the sample surface. Iron-rich intermetallics have segregated mainly at the eutectic grain boundaries (region C). The microstructure of the Sr-modified alloy after 120 min of melt holding is similar to that of the unmodified alloy, see Fig. 1(c). The eutectic Si exhibits a coarse lamellar morphology, which is typical for an unmodified eutectic microstructure. Iron-rich intermetallics are hardly visible.

3.2. FIB-EsB tomography

Figure 2 demonstrates a typical SEM-EsB image of the eutectic microstructure of the unmodified alloy. Phases of different gray scale levels are clearly visible. Apart from the two main eutectic components Al and Si, additional intermetallic impurity phases can be identified owing to the contrast provided by the EsB detector, and their specific morphology. Several small-scale intermetallic impurity particles are less than 500 nm in size (marked by arrows in Fig. 2) so that they can hardly be distinguished from the unmodified eutectic Si plates by observations that provide only morphological information. In order to identify the elements present in the light gray phases, the chemical composition was measured by SEM-EDX on FIB slices. The phases with brighter contrast contained mainly Fe and the additional impurity elements present in the alloys investigated. Eutectic Si plates as well as Fe-rich intermetallics are embedded in the eutectic Al matrix. Within the eutectic Al, the contrast slightly varies due to different crystallographic orientations of individual Al grains.

The 3D microstructure of the unmodified eutectic Si is shown in Fig. 3. The Si plates are interconnected and are branched, thus forming a lamellar Si network. The observed thickness of lamellar Si plates is 250-800 nm (measured in the xy-imaging plane ±50 nm). Iron-rich intermetallics are attached to the Si plates, but not necessarily to one of the edges of the plates as reported previously [21]. One part of the Fe-rich intermetallics with sizes below 500 nm exhibits nearly spherical morphology. The other part exhibits 'Chinese script' morphology. The term 'Chinese script' has been commonly used to characterize certain Fe-rich intermetallics in 2D sections [22]. It is observed that these Fe-rich intermetallics are precipitated as inclusions between the Si plates and the eutectic Al matrix. They are uniformly distributed and can be up to 6 μm long. A separate 3D visualization of the Fe-rich intermetallics is shown in Fig. 3(b). The fine 3D morphology of such intermetallic phases was previously described as convoluted branched structure [14]. The intermetallic phases in the present study form thin flat sheets aligned along the surfaces of the Si plates and often connect different Si plates along the interfaces of two eutectic Al grains. The estimated volume fractions of eutectic Si and intermetallic phases are 13.6 vol% and 0.3 vol%, respectively.

Site-specific FIB-EsB tomography of the Sr-modified alloy after 5 min of melt holding was performed in both regions B and C as indicated in Fig. 1(b). The 3D morphology of the eutectic Si in region B is visualized in Fig. 4(a). A partially modified microstructure which appears as a mixed structure of thin Si platelets and fibrous Si is observed. This fine fibrous morphology is often described as seaweed- or coral-like structure [15, 23]. The eutectic Si fibers are interconnected and form a highly branched network. The estimated volume fraction of eutectic Si is about 12 vol% within the volume investigated. SEM-EsB images of this region reveal no contrast from intermetallic phases, which indicates that Fe-rich intermetallics or additional intermetallic impurity phases are not present. Figure 4(b) visualizes in 3D a Fe-rich phase segregation with ‘Chinese script’ morphology found in region C of Fig. 1(b). Beside this phase a further needle-shaped Fe-rich phase is observed at the eutectic grain boundaries (not shown here). The Fe-rich intermetallics in Fig. 4(b) are clustered to an interconnected network. They are much larger than in the unmodified alloy. Additional intermetallic phases of other impurity elements appear as very bright spots within the Fe-rich network. These impurities (white in Fig. 4(b)) are attached either to the eutectic Si or to the Fe-rich intermetallics and are globular with diameters up to 700 nm.

Figure 5 shows a selected volume of the Sr-modified Al-15Si sample after 120 min of melt holding. This volume has been selected to display the interfaces between plates of eutectic Si and Fe-rich intermetallics. It is evident from Fig. 5(a) that after 120 min of melt holding the eutectic Si exhibits the plate-like morphology characteristic for the unmodified state. The Fe-rich intermetallics occur in close contact with plates of eutectic Si. The estimated volume fraction of eutectic Si is 12.5 vol% in the entire investigated volume of $21.2 \times 8.6 \times 10.2\ \mu m^3$. The Fe-rich intermetallics are distributed similar to those in Fig. 3(b). However, no small-scale Fe-rich particles are visible and the size of the Fe-rich intermetallics with ‘Chinese script’ morphology is increased as shown in Fig. 5(b). Globular intermetallic impurity phases are found either attached to the Fe-rich intermetallics or located right next to unmodified Si plates. Typical Fe-rich intermetallic particle lengths range from 2.5 to 6.5 μm. The volume fraction of the intermetallic impurities within the eutectic is increased to about 0.75-1.0 vol %.

3.3. Identification of intermetallic phases

Iron-rich and other intermetallic impurity phases appear darker than both the surrounding Al matrix and the eutectic Si in the TEM due to atomic number contrast. They can therefore be easily identified. The analysis of the phases observed is given in Table 2.

One of the Fe-rich intermetallics is imaged using bright field TEM in Fig. 6(a). The corresponding SAED pattern is displayed in Fig. 6(b). The structure of such phases was found body-centered cubic, space group Im3, with a lattice parameter a=1.271 nm. The average chemical composition of this phase as given in Table 2 indicates a stochiometry of $Al_{12}(Fe, Mn)_4Si_2$.

SEM-EsB images of platelet-shaped Fe-rich phases in the Sr-modifed alloy after 5 min of melt holding are presented in Fig. 7. The image in Fig. 7(a) was taken in region C of Fig. 1(b). Several platelets are segregated at the eutectic grain boundaries. On average, the depicted platelets are about 4 μm long. From those platelets samples for TEM were prepared, see Fig. 7(b). In order to find the features of interest in region C in electron-transparent areas the TEM lamella was first imaged by SEM-EsB, after which the platelet marked by an arrow in Fig. 7(b) was analysed by TEM. We find a tetragonal unit cell corresponding to the $PdGa_5$-structure with the lattice parameters a=0.614 nm, c=0.957 nm, which is in accordance with the Al_3FeSi_2-phase observed in Ref. 24.

The representative SEM-EsB image of the Sr-modified Al-Si eutectic after 120 min of melt holding presented in Fig. 8(a) exhibits compositional gray scale levels corresponding to several phases and crystallographic orientations of the eutectic Al matrix. The phase with the brightest contrast corresponds to the impurities found in both Sr-modified alloys after 5 and 120 min of melt holding. They precipitate as small spherical particles close to either the Fe-rich intermetallics or the Si plates. Figure 8(b) shows a bright field TEM image of a typical Fe-rich phase with another intermetallic impurity phase attached. The EDX spectrum from the globular particle, labelled by the arrow in Fig. 8(b), indicates a formation of mainly Pb. The diffraction pattern of the Fe-rich intermetallic phase (Fig. 8(c)) was again found to match a body-centered cubic unit cell with a=1.245 nm. The EDX spectra obtained from the Fe-rich phase indicate a stochiometry of $Al_{16}(Fe, Mn)_5Si_2$.

4. Discussion

4.1. Formation of unmodified microstructure

An identification of Fe-rich intermetallics merely based on their morphology can be misleading because different phases can have similar morphologies, as has been previously reported in Ref. 25. Therefore, an identification of Fe-rich intermetallics was carried out by both structure determination and composition analysis in this work. The intermetallic phase $Al_{12}(Fe,Mn)_4Si_2$ (Table 2) found in the unmodified alloy is suggested to be an α-type Al(Fe,Mn)Si phase [26]. A stable equilibrium phase of similar composition (32.5 wt% Fe and up to 10.5 wt% Si) has been identified as α-Al(Fe,Mn)Si phase [27]. Many phases containing different levels of Fe and Mn are known in the literature as 'α-Al(Fe,Mn)Si phase'. Although the chemical compositions of the reported phases are slightly different the lattice parameters are nearly the same, about a=1.245 nm, as for α-$Al_{15}(Fe,Mn)_3Si_2$ [26, 28]. This indicates that the range of homogeneity of the Fe-rich α-phase is much wider than suggested by the phase diagram proposed in [29].

The 3D visualization of the unmodified eutectic microstructure in Fig. 3 clearly indicates an uniform distribution of the Fe-rich α-phase. Due to the low Fe level present in the investigated alloys, these Fe-rich intermetallics have solidified after the main eutectic Al-Si reaction. Based on FIB-EsB tomography, it is proposed that the evolution of the 3D morphology of the Fe-rich α-phase during eutectic growth proceeds according to the model illustrated schematically in Fig. 9.

Figure 3(a) suggests that the eutectic Si forms an interconnected plate-like network. Due to the branching of Si plates, melt enriched in alloying elements is trapped in isolated pockets between adjacent Si plates. Consequently, eutectic Al nucleates and grows on the Si plates in regions with higher Al concentration, see Fig. 9(a). Similar ideas about cooperative Al-Si eutectic growth provided by repeated epitaxial nucleation of eutectic Al on Si plates and the formation of polycrystalline Al grains have been reported [30–32]. As eutectic solidification proceeds, the melt enriches in Fe due to the rejection of Fe at the solid-liquid interfaces, see Fig. 9(b). Since the Fe-rich α-phase is often observed between two Si plates in their growth direction (see arrows in Fig. 9(b)), it can be concluded that Fe enriches preferentially at the growth front of the Al-Si eutectic. The nucleation of the Fe-rich α-phase finally takes place in regions with higher Fe concentration. The shape of the Fe-rich α-phase is strongly correlated to both the flat Si interface and the interfaces of the polycrystalline Al matrix. Therefore, the final 3D morphology of the Fe-rich α-phase is determined on the one hand by the flat Si interface and on the other by the necking caused by the growing polycrystalline Al-Al interfaces, see Fig. 9(c). This leads to the solidifcation of Fe-rich α-phase as thin sheets between the eutectic Si-Al and Al-Al interfaces.

Recently, it has been shown that several oxides may be suitable nucleant substrates for intermetallic phase formation [33]. However, in the present study no features related to oxide films or bifilms were observed in the vicinity of the Fe-rich α-phase. Furthermore, there is no indication that the morphology of the Fe-rich α-phase is given by precipitation and growth around bifilms.

4.2. Alloy after 5 min of melt holding

The addition of Sr and 5 min of melt holding affects the formation of the eutectic phases. To achieve a fully modified structure in hypoeutectic alloys the level of Sr is generally in the range of about 80-120 ppm [34]. Due to the lower Sr level (62 ppm) observed after 5 min of melt holding in the investigated hypereutectic alloy and its high eutectic volume fraction, it is expected that locally the modification effect could be lost or be incomplete. Indeed, areas with modified and unmodified microstructure can be obtained, see Fig. 1(b). Therefore, the microstructure of the Sr-modified alloy after 5 min of melt holding is less homogenous than that of the unmodified alloy.

The Sr level of 62 ppm not only refines the eutectic Si but also changes the size and morphology of the Fe-rich intermetallics. As seen in region C of Fig. 1(b), the addition of Sr results in a local segregation of the Fe-rich intermetallics at the eutectic grain boundaries, where finally complex intermetallic phases have solidified. The location of the intermetallic phases at the modified eutectic grain boundaries as observed in the present work is in accordance with reported results and the predicted microstructure in the final stages of eutectic grain growth [17]. In the present study, two different morphologies of Fe-rich intermetallics were observed at the location of impingement of boundaries between modified eutectic grains (region C of Fig. 1(b)).

First, the Fe-rich phase shown in Fig. 4(b) is suggested to be a Fe-rich α-phase because of its similarity of morphology and chemical composition with the Fe-rich α-phase in the unmodified alloy. The Fe-rich α-phase exhibits a coarse dendritic or so-called 'Chinese script' morphology in individual 2D images that are composed to a 3D image in Fig. 4(b). In 3D, however, the shape of the Fe-rich α-phase no more resembles a 'Chinese script' but appears as branched sheets in an interconnected network. 'Chinese script' is therefore merely a description of a 2D section of a more complex 3D object.

Thin platelet-shaped Fe-rich phases (second type of morphology) which appear as needles in the 2D microstructure have also been found at the eutectic grain boundaries. The chemical composition of these Fe-rich platelets is listed in Table 2 and corresponds to $Al_{3.3}Fe_{1.3}Si_2$. Their tetragonal structure (a=0.614 nm, c=0.957 nm) as well as their chemical composition are similar to that of the reported Al_3FeSi_2-phase [24]. This phase has been previously designated δ-phase [35]. The small difference in the lattice parameter to the literature can be explained by a slight composition deviation from the reported Fe-rich δ- phase. The formation of Fe-rich δ-phase in our Al-15Si alloy (cooling rate 6-7 K/s) conforms with the prediction of such a phase in alloys with high contents of Si, especially at high melt cooling rates [35]. Iron-rich intermetallics with platelet morphology are often misleadingly identified as β-Al_5FeSi [25]. However, the Fe-rich β-phase was not found in the alloys investigated, since their Fe level is too low. In addition, it is known that the presence of Mn prevents the formation of the Fe-rich β-phase [36].

The additional intermetallic impurity phases containing Pb (white spots in Fig. 4(b)) are clearly visible in the FIB-EsB images due to strong imaging contrast. They are also segregated within the Fe-rich phase network at the eutectic grain boundaries. There is no evidence that these globular particles act as heterogenous nucleation sites for the Al-Si eutectic or Fe-rich intermetallics.

Figure 4(a) reveals a mixed structure of thin Si platelets and fibrous Si, indicating a gradual transition of the structure from coarse Si plates into finer fibers. In addition, no intermetallic impurity phases have been found in the fibrous modified Si network, see Fig. 4(a). The absence of intermetallic impurities in the modified eutectic regions has not been reported previously. The difference in size and distribution of the Fe-rich intermetallics can be understood by the evolution of a very smooth eutectic growth front during solidification in Sr-modified alloys [37]. Therefore, the last liquid pockets in which the Fe-rich intermetallics finally solidify are exclusively located at the eutectic grain boundaries.

4.3. Alloy after 120 min of melt holding

As Sr is a slowly acting modifier showing an incubation period of one to two hours [6, 38–40] the melt holding time of 120 min in the present work was chosen to check the limits of the modification effect. No effect of modification after melt holding for 120 min could be observed anymore. The chemical composition of the alloy as shown in Table 1 reveals that practically no Sr is contained in the alloy. Sr has been most likely lost by oxidation during melt holding. The eutectic morphology of the Al-15Si alloy is changed back to an unmodified plate-like eutectic Si.

The microstructure of the Fe-rich α-phase is comparable with that of the unmodified alloy, but the Fe-rich α-phase found here is less uniformly distributed and appears mainly as attachment to Si plate surfaces with an increased particle size. The local volume fraction of the Fe-rich intermetallics is increased from 0.3 vol% ($\widehat{=}$ 0.15 wt% Fe) for the unmodified alloy up to 1.0 vol% ($\widehat{=}$ 0.44 wt% Fe) for the Sr-modified alloy held for 120 min. Since the Fe present in the unmodified alloy is completely precipitated in Fe-rich intermetallics (0.15 wt% Fe, see Table 1), the locally measured volume fraction of up to 1.0 vol% for the alloy after 120 min of melt holding can only be explained by an inhomogeneous distribution of the Fe-rich intermetallics. The lack of small-scale Fe-rich intermetallics and their coarsening are most likely caused by extended melt holding.

5. Summary

Using FIB-EsB tomography with a resolution of $\leq$ 50 nm it was possible to obtain compositional contrast and hence to visualize in three dimensions the shape and morphology not only of eutectic Si but also of intermetallic impurity phases in unmodified and Sr-modified Al-15Si alloys. A model for the evolution of the 3D morphology of the Fe-rich α-phase in the unmodified alloy is proposed. The addition of Sr modifies the morphology of eutectic Si from a plate-like network for the unmodified alloy to a fine fibrous structure in the Sr-modified alloy after 5 min of melt holding. No Fe-rich intermetallics were observed within the fine fibrous structures of modified eutectic Si. The

Fe-rich bcc α-phase within the eutectic microstructure of the unmodified alloy coarsens to interconnected sheets and segregates to the eutectic grain boundaries. In addition, tetragonal Fe-rich δ-phase platelets were observed at the eutectic grain boundaries.

After 120 min of melt holding, the Sr-modified alloy exhibits a eutectic Si morphology as for unmodified alloys. The Fe-rich bcc α-phase is coarser than in the unmodified alloy. Whereas the Fe-rich α-phase appears in both unmodified and Sr-modified alloys, Fe-rich δ-phases only occurred in the Sr-modified alloy after 5 min of melt holding.

Acknowledgments

The authors would like to thank Mr. R. Grothausmann for the fruitful discussions on 3D image processing. We also gratefully acknowledge the alloy preparation by Dr. A.K. Prasad Rao and Dr. G.S. Vinod Kumar.

References

[1] Gruzleski JE. AFS Trans 1992;100:673–83.

[2] Mondolfo LF. J Aust Inst Met 1965;10:169–77.

[3] Lu SZ, Hellawell A. Metall Mater Trans A 1987;18:1721–33.

[4] Nogita K, McDonald SD, Dahle AK. Mater Trans 2004;45:323–6.

[5] Couture A. Int Cast Met J 1981;6:9–17.

[6] Bäckerud L, Chai G, Tamminen J. Solidifcation Characteristics of Aluminum Alloys; vol. 2. Stockholm: AFS/Skanaluminium; 1990.

[7] Khalifa W, Samuel FH, Gruzleski JE. Metall Mater Trans A 2003;34:807–25.

[8] Shabestari SG, Gruzleski JE. AFS Trans 1995;26:285–93.

[9] Mulazimoglu MH, Tenekedjiev N, Closset B, Gruzleski JE. Cast Metals 1993;6:16–28.

[10] Samuel FH, Samuel AM, Doty HW, Valtierra S. Metall Mater Trans A 2001;32:2061–75.

[11] Lu L, Dahle AK. Metall Mater Trans A 2005;36A:819–35.

[12] Khalifa W, Samuel A, Samuel F, Doty H, Valtierra S. Int J Cast Metal Res 2006;19:156–66.

[13] Dinnis CM, Dahle AK, Taylor JA. Mat Sci Eng A 2005;392:440–8.

[14] Dinnis CM, Taylor JA, Dahle AK. Scripta Mater 2005;53:955–8.

[15] Lasagni F, Lasagni A, Marks E, Holzapfel C, Mücklich F, Degischer HP. Acta Mater 2007;55:3875–82.

[16] Schaffer M, Wagner J, Schaffer B, Schmied M, Mulders H. Ultramicroscopy 2007;107:587–97.

[17] McDonald S. Eutectic solidification and porosity formation in unmodified and modified hypoeutectic aluminium-silicon alloys. Ph.D. thesis; 2002.

[18] Holzer L, Indutnyi F, Gasser PH, Münch B, Wegmann M. J Microsc-Oxford 2004;216:84–95.

[19] Thevenaz P, Ruttimann UE, Unser M. IEEE Trans Image Process 1998;7:27–41.

[20] Zhang H. Thin Solid Films 1998;320:77–85.

[21] Shankar S, Riddle YW, Makhlouf MM. Acta Mater 2004;52:4447–60.

[22] Crosley PB, Mondolfo LF. AFS Trans 1966;74:53–64.

[23] Dahle AK, Nogita K, Zindel JW, McDonald SD, Hogan LM. Metall Mater Trans A 2001;32:949–60.

[24] Gueneau C, Servant C, Dyvoire F, Rodier N. Acta Cryst C 1995;51:177–9.

[25] Kral MV. Mater Lett 2005;59:2271–6.

[26] Cooper M. Acta Cryst 1967;23:1106–7.

[27] Pratt JN, Raynor GV. J Inst Metals 1951;79:211–32.

[28] Dons AL. Z Metallkde 1985;76:151–3.

[29] Shabestari SG. Mat Sci Eng A 2004;383:289–98.

[30] McLeod AJ, Hogan LM, Adam CM, Jenkinson DC. J Cryst Growth 1973;19:301–9.

[31] Shamsuzzoha M, Hogan LM. J Cryst Growth 1986;76:429–39.

[32] Hogan LM, Song H. Acta Metall 1987;35:677–80.

[33] Cao X, Campbell J. Mat Sci Eng A 2003;34A:1409–20.

[34] Sigworth GK. Int J Metalcast 2008;2:19–41.

[35] Mondolfo LF. Aluminum alloys: structure and properties. London: Butterworth; 1976.

[36] Mondolfo LF. Manganese in Aluminium Alloys. Neuilly Sur Seine, France: Manganese Centre; 1978.

[37] Kobayashi KF, Hogan LM. J Mater Sci 1985;20:1961–75.

[38] Tsumura Y, Sakakibara A, Toyoda K, Ishikawa M. J Jpn Inst Light Metals 1980;30:239–45.

[39] Hess PD, Blackmun EV. Giesserei-Praxis 1976;8:115–9.

[40] Chai G, Bäckerud L. AFS Trans 1992;100:847–54.

Tables

Table 1: **Iron concentration (in wt%) and additional impurity levels (in ppm) of the Al-15Si alloys investigated. The samples used for chemical analysis were taken from the solidified castings.**

Alloy	Fe	Al-Si	Cu	Mn	Mg	Zn	Ga	Pb	Sr
	wt%		ppm						
Unmodified	0.152	Balance	22	64	2	30	171	<1	<1
Sr, 5 min	0.165	Balance	73	116	11	159	167	75	62
Sr, 120 min	0.165	Balance	75	118	<1	161	167	79	<1

Table 2: **Average composition of Fe-rich intermetallics (in at%) measured by energy dispersive spectroscopy in the transmission electron microscope. The morphology of intermetallic phase known as 'Chinese script' in 2D corresponds to the branched sheet-shaped morphology observed in 3D.**

Alloy	Phase	3D Morphology	Al	Si	Fe	Mn	Mg
			at%				
Unmodified	α	Thin sheets	66.9	11.5	21.1	0.5	-
Sr, 5 min	α	Branched sheets*	69.1	7.7	22.6	0.6	-
	δ	Platelets	48.8	27.3	20.3	0.4	3.2
Sr, 120 min	α	Thin sheets	71.2	8.9	19.1	0.8	-

*Measured in the scanning electron microscope (10 kV).

Figures

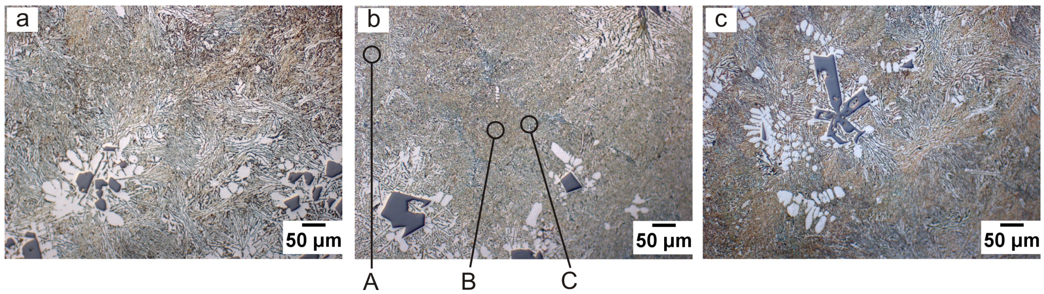

Figure 1: Optical micrographs taken from the (a) unmodified and Sr-modified castings after (b) 5 min and (c) 120 min of melt holding. The micrographs were obtained by differential interference contrast. In (b) three regions with different microstructural features are labelled: unmodified eutectic microstructure (region A), modified eutectic microstructure (region B), location of impingement of eutectic grain boundaries (region C).

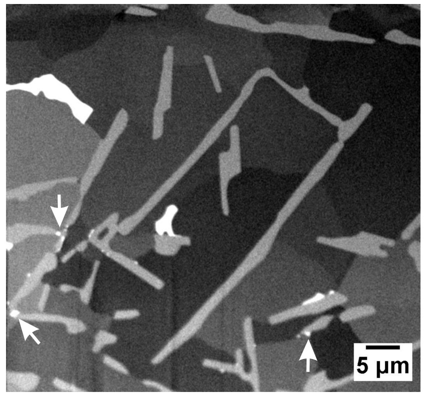

Figure 2: Microstructure of unmodified Al-15Si alloy: SEM-EsB image of the eutectic microstructure with different compositional gray scale levels (black=Al, dark gray=Si, light gray=Fe-rich). Some small-scale Fe-rich intermetallics are marked by arrows.

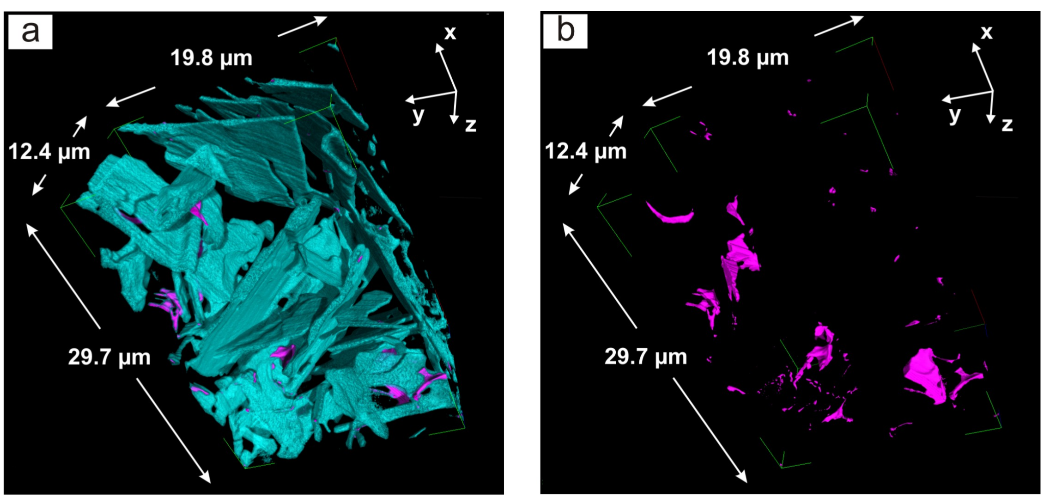

Figure 3: (a) 3D morphology of eutectic Si (in cyan) and Fe-rich intermetallics (in magenta) of the unmodified alloy. (b) Fe-rich intermetallics visualized without the adjacent Si plates.

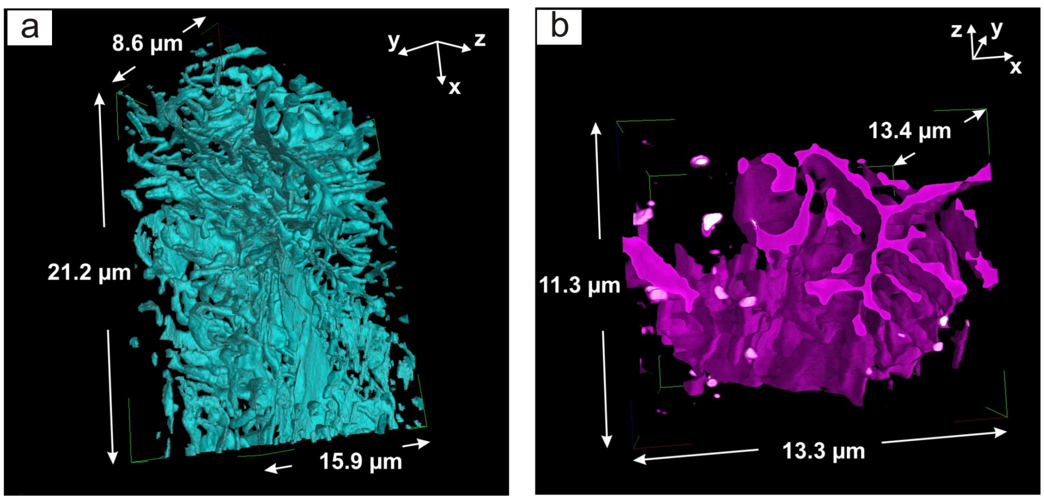

Figure 4: (a) 3D morphology of eutectic Si and (b) Fe-rich intermetallics of the Sr-modified Al-15Si e after 5 min of melt holding. The partially modified Si morphology in (a) was observed in region B of Fig. 1(b). Note that no Fe-rich intermetallics are present in the modified eutectic microstructure. The segregated Fe-rich intermetallics in (b) were observed at the eutectic grain boundaries in region C of Fig. 1(b). The globular white features in (b) correspond to additional intermetallic impurity phases.

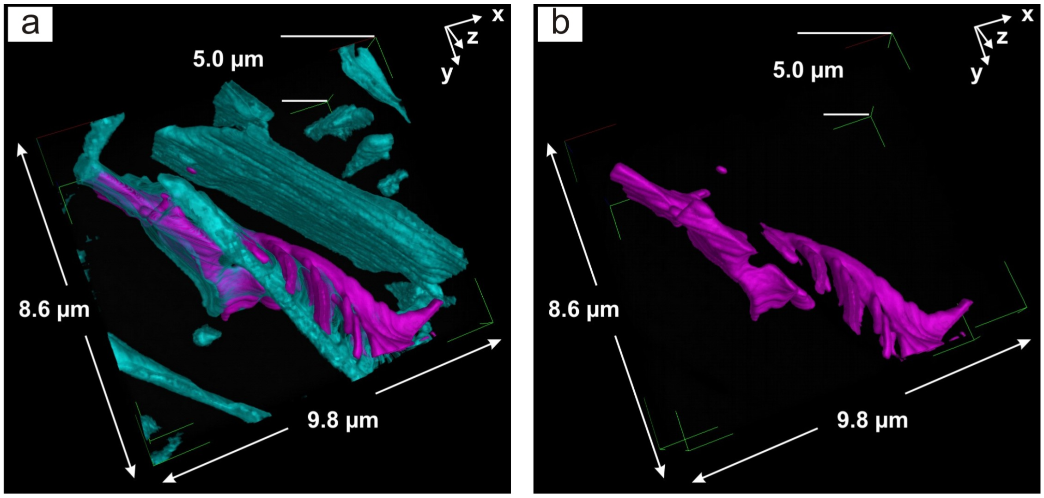

Figure 5: (a) 3D morphology of eutectic Si (in cyan) and Fe-rich intermetallics (in magenta) of the Sr-modified Al-15Si alloy after 120 min of melt holding. (b) Fe-rich intermetallic phase visualized without the adjacent Si plates.

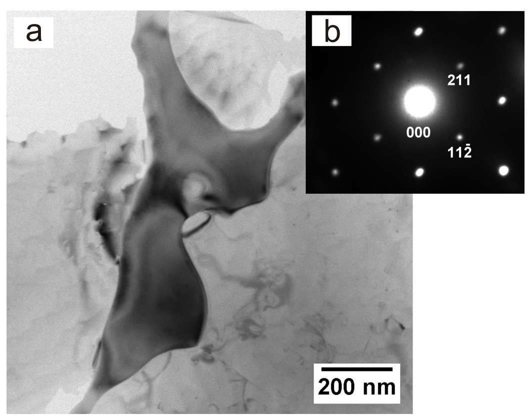

Figure 6: Microstructure of unmodified Al-15Si alloy. (a) Bright-field TEM image of a Fe-rich intermetallic particle with 'thin sheet' morphology, corresponding to the Fe-rich intermetallic phase shown in Fig. 2. (b) SAED pattern of the Fe-rich α-phase along the $[3\bar{5}\bar{1}]$ zone axis.

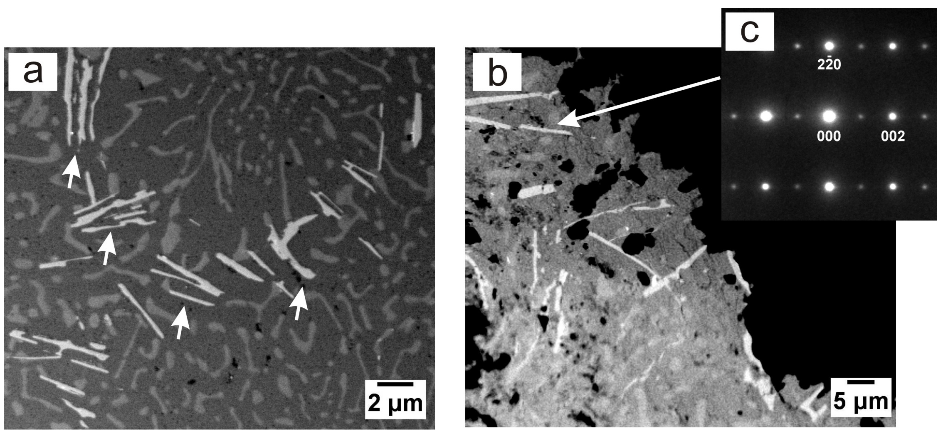

Figure 7: SEM-EsB images of Sr-modified Al-15Si alloy after 5 min of melt holding: (a) EsB image of the microstructure shows Fe-rich δ-phase with platelet morphology from region C in Fig. 1(b). (b) EsB image of specimen prepared for TEM investigation. The white arrow indicates the specific platelet analysed in TEM. (c) SAED pattern obtained from the Fe-rich δ-platelet along the [110] zone axis.

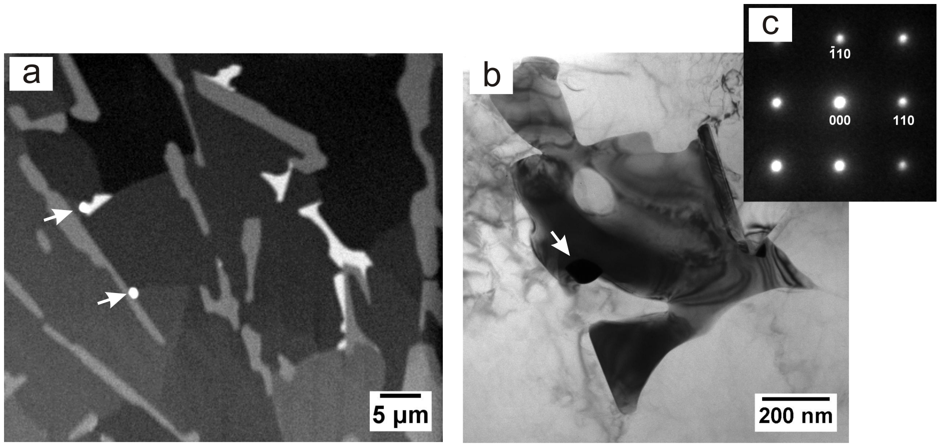

Figure 8: Microstructure of Sr-modified Al-15Si alloy after 120 min of melt holding: (a) SEM-EsB image of eutectic microstructure revealing different intermetallic impurity phases marked by arrows. (b) Bright-field TEM image of Fe-rich α-phase with additional intermetallic impurity phase attached (indicated by arrow). (c) SAED pattern of the Fe-rich α-phase along [001] zone axis.

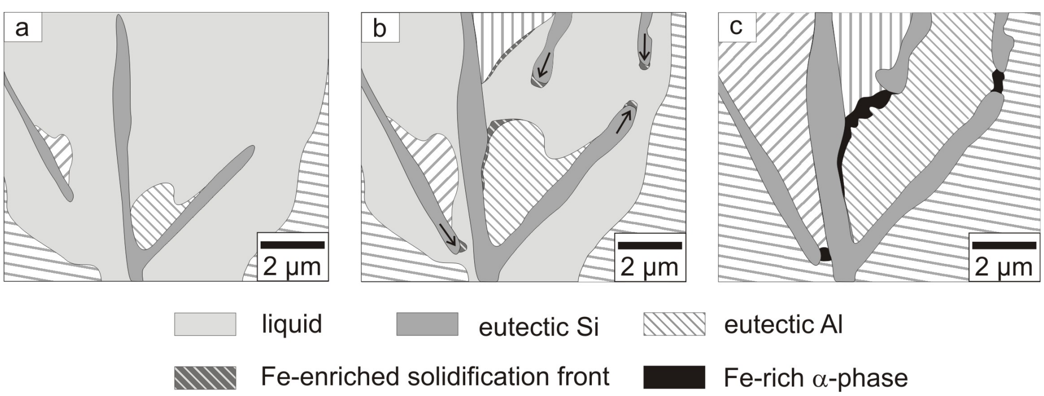

Figure 9: Schematical 2D illustration of the 3D morphology formation of the Fe-rich α-phase present in the unmodified Al-Si eutectic microstructure. The arrows in (b) illustrate the growth direction of the Si plates.